Effect of the acidic strength on the vapor phase Beckmann rearrangement of cyclohexanone oxime over the MFI zeolite: an embedded ONIOM study†

Jakkapan Sirijaraensre[ab] and Jumras Limtrakul*[ab]

Received 22nd May 2008, Accepted 7th October 2008
First published as an Advance Article on the web 5th November 2008
DOI: 10.1039/b808662a

The mechanism and energetic profile of the Beckmann rearrangement reaction of cyclohexanone oxime to ε-caprolactam catalyzed by the H-[Al]-MFI and H-[B]-MFI zeolites were investigated by both the bare cluster and the ONIOM models at the B3LYP/6-31G(d,p) and the B3LYP/6-31G(d,p) : MNDO levels of theory, respectively. In order to improve the energetic properties and take into account the whole zeolite framework effect, single point calculations are undertaken at the embedded ONIOM2 schemes; MP2/6-311G(d,p) : HF/6-31G(d) with an additional long-range electrostatic potential from the extended zeolite framework. The reaction mechanism of the Beckmann rearrangement over the acid site of zeolites consists of three steps: the 1,2 H shift, the rearrangement and the tautomerization. The activation energies for the Beckmann rearrangement of cyclohexanone oxime on the H-[Al]-MFI zeolite are calculated to be 31.46, 16.15 and 18.95 kcal mol^{-1}, for the first, second and third steps, respectively, whereas in the H-[B]-MFI zeolite, the energy barriers for each step of the reaction are 24.33, 7.46 and 20.43 kcal mol^{-1}, respectively. The rate-determining step of the reaction is the first step, which is the transformation from the N-ended cyclohexanone oxime adsorption complex and the O-ended one. These results signify the important role that the acid strength of zeolites plays in altering the energy profile of the reaction. The results further indicate that the weak Brønsted acid sites in the [B]-MFI zeolite could better catalyze the Beckmann rearrangement of cyclohexanone oxime than the strong acid sites in the [Al]-MFI zeolite, as compared with the quantitatively low activation energy of most steps. However, the turnover reaction of the H-[B]-MFI zeolite might be delayed by the quantitatively high desorption energy of the product as compared to the adsorption energy of the reactant.

Introduction

The Beckmann rearrangement[1–6] is one of the most important industrial reactions for producing the ε-caprolactam, an important intermediate for the production of the Nylon-6 polymer. In the conventional method, this process uses acid solution, ammonia and cyclohexane as the principal raw materials. However, it is both environmentally unfavorable; due mainly to the use of corrosive sulfuric acid, instrument corrosion occurs and wastes the resources; and ammonium sulfate, a by-product formed during the neutralization process, is produced at approximately 1–5 times that of ε-caprolactam. Hence, a range of heterogeneous catalysts are used in this reaction with the objective of overcoming these problems. Zeolites have been widely investigated on this reaction, for example MFI,[7–16] FAU,[15–20] Beta,[20–25] and MOR[15,16,20] zeolites. From previous studies, it is of interest to note that porous catalysts like zeolites show both high activity and provide a highly selective product. As a result of these investigations, Sumitomo Chemical Co., Ltd., have industrialized the production of ε-caprolactam, using high-silica MFI zeolite as the catalyst for the vapor phase Beckmann rearrangement. This process does not produce any ammonium sulfate, a by-product through the Beckmann rearrangement without a catalyst.

The Beckmann rearrangement catalyzed by solid catalysts (usually called the vapor-phase Beckmann rearrangement) has been the subject of many researchers who have developed suitable experimental and computational techniques for finding an efficient catalyst which can enhance the process of manufacturing the desired product. In earlier studies,[18,19,23,26,31] strong Brønsted acid sites in zeolites were suggested as playing a crucial role in catalyzing this reaction by protonating the oxime molecule, whereas external silanols appear to be nonreactive, while in some previous works,[8,11,12,21,32,33] they have reported that the weak acidic groups in zeolites such as high-silica MFI, [B]-MFI and [B]-Beta are also active catalysts for the rearrangement reaction with high activity and selectivity toward ε-caprolactam.

[a] *Laboratory for Computational and Applied Chemistry, Chemistry Department, Faculty of Science, Kasetsart University, 10900 Bangkok, Thailand. E-mail: fscijrl@ku.ac.th*
[b] *Center of Nanotechnology, Kasetsart University Research and Development Institute, Kasetsart University, 10900 Bangkok, Thailand. E-mail: fscijrl@ku.ac.th*

† Electronic supplementary information (ESI) available: Additional experimental details. See DOI: 10.1039/b808662a

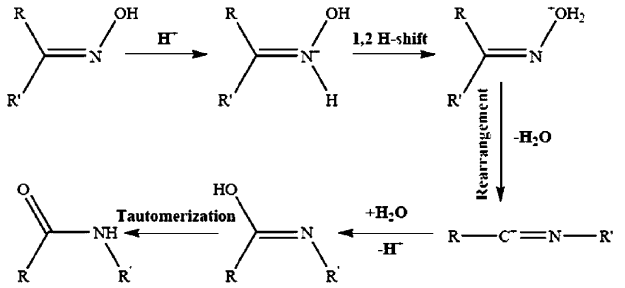

Scheme 1 The reaction mechanism for the Beckmann rearrangement.

Therefore, the role of the acid site strength in the Beckmann rearrangement is a matter of debate.

The reaction mechanism over the Brønsted acid site of zeolite catalysts is intensively investigated both experimentally[22,23,34–36] and theoretically.[26–28,36,37] The reaction mechanism, commonly suggested for the Beckmann rearrangement, is described in Scheme 1 as follows:

The reaction initially involves the protonation of the oxime molecule at the nitrogen atom of the oxime molecule (designated by N-Bound). Then, in the first TS step, named the 1,2 H-shift step, the hydrogen is transferred from the nitrogen-end to the oxygen atom of the oxime molecule (designated as O-Bound) and followed by migration of an R group (R = alkyl, aryl or hydrogen), which is *anti* to both the hydroxyl group and to the nitrogen atom, and a water molecule is displaced. This second step is called the rearrangement step. Subsequently, the displaced water molecule binds to the carbon atom, simultaneously transferring a proton to the acid catalyst. The last transforming step is the tautomerization from the enol–amide complex to the amide complex and desorption of the amide molecule in the final step. Recently, theoretical investigations reveal that the transfer of proton from the nitrogen-end to the oxygen-end of oxime molecules is the rate-determining step of the reaction when it occurs over zeolite catalysts. Nevertheless, the theoretical investigation of the Beckmann rearrangement on zeolite systems is not yet well-founded.

The aim of this work is to investigate the effect of the Brønsted acid site strength in isomorphously substituted MFI zeolites: H-[Al]-MFI and H-[B]-MFI zeolites, on the reaction mechanism and the energetic profile of the Beckmann rearrangement of cyclohexanone oxime. To the best of our knowledge, no theoretical study has investigated the Beckmann rearrangement mechanism of cyclohexanone oxime catalyzed by as large a unit cell zeolite as MFI zeolite. This finding can provide more insight into the role of the acidic strength of zeolite on the Beckmann rearrangement reaction. The interaction of the MFI zeolite and the oxime molecule has been investigated by using the bare cluster and embedded ONIOM approaches.

Computational details

To determine the adsorbed structure of cyclohexanone oxime molecules in H-[Al]-MFI and H-[B]-MFI zeolites, the ONIOM models were used. The T12 site, which has been widely used to model the active site of MFI in many theoretical studies, is substituted with two different types of trivalent atoms; Al^{3+} and B^{3+}. Either B substitution or Al substitution introduces a net negative charge in the zeolite framework which is compensated by a proton acting as a Brønsted acid site to preserve neutrality. Due mainly to the large unit cell of the MFI zeolite, the use of periodic calculation is computationally too expensive and even impractical. Recently, hybrid methods such as the embedded cluster,[26,27,38–46] QM-Pot[47–49] as well as the ONIOM methods[50–59] have been used for including the framework effects of zeolite with the benefit of the computational cost becoming economically feasible. In the ONIOM2 scheme, the MFI zeolite is represented by the 128T model which covers the nanometer-sized cavity that is the intersection of the main and sinusoidal channels and the location of the active site of MFI zeolite. The 128T ONIOM model (see Fig. 1) is divided into two layers: only the small active region (12T) located at the intersection of the main and sinusoidal channel is accessible to the adsorbates (see Fig. 1a–b), the active site of the H-MFI zeolite was treated accurately with the density functional theory (B3LYP) with the 6-31G(d,p) basis set, while the contribution of influences from the rest of the model was approximated by a less expensive method (MNDO). This combination was previously used to investigate the adsorption of NH_3 and H_2O in H-CHA zeolite.[59] These results showed that the adsorbed structures obtained from the ONIOM2(B3LYP : MNDO) scheme are in agreement with those obtained from periodic calculations. In order to obtain more accurate adsorption energies, single point calculations were carried out at the ONIOM2(MP2/6-311G(d,p) : HF/6-31G(d)) level of theory. Attempts have been made to demonstrate that the geometry constraints imposed in this work do not influence the results. Some test calculations on cyclohexanone oxime over the H-[Al]-MFI and H-[B]-MFI zeolite have been performed using two different sizes of QM region: 12T and 30T atoms with a different degree of relaxation in QM regions (see ESI, Fig. S1 and Table S1).† It was found that no significant structural differences were obtained when using 5T, 8T and 24T clusters during optimization. Furthermore, the combination of B3LYP and UFF, which has shown good results in predicting the structural parameters and reaction energies in previous works, is preformed to compare the results with the MNDO environment. The B3LYP : UFF combination[60–65] has been found to provide a good description of the short range van der Waals

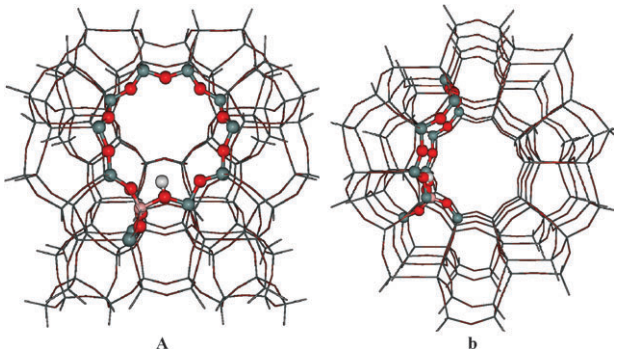

Fig. 1 Presentation of the 128T ONIOM2 model of H-MFI zeolite. The atoms belonging to the high-level region are presented as bonds and sticks, while the rest of the atoms belong to the low-level region.

interactions. The ONIOM calculation using B3LYP : MNDO with the 12T : 128T cluster leads to geometry similar to that obtained from the B3LYP : UFF calculations. The adsorption energy computed from MP2/6-311G(d,p) : HF/6-31G(d) single point calculations at the B3LYP/6-31G(d,p) : MNDO optimized structures, is also in agreement with the B3LYP : UFF value. Consequently, the use of the MP2/6-311G(d,p) : HF/6-31G(d)//B3LYP/6-31G(d,p) : MNDO approach seems to be a good strategy to model this system (see ESI, Table S2).† All optimizations have been preformed on the 12T/5T cluster embedded in the 116T cluster treated by the MNDO method. However, the 128T ONIOM model neglects the long-range effects from the remaining infinite lattice of zeolite (excluding the 128T ONIOM model). Hence, in order to fulfil the entire behavior of the adsorption properties of the probe molecule in the zeolite pore, the ONIOM model is embedded in the zeolitic Madelung potential field which is represented by two sets of point charges generated by the SCREEP method.[26,27,40–46] The detailed description of the SCREEP method which reproduces the correct Madelung potential calculated from the Ewald-sum method was previously reported elsewhere.[38,40] This new model can take into consideration the long-range effects extended from the general ONIOM model. The combination of the SCREEP and ONIOM approach is called the embedded-ONIOM approach (e-ONIOM) which is a sufficiently accurate and practical model for studying reaction mechanisms on zeolite systems.[64,66,67] Verification that the optimized transition state connects the intended reactant and product, was made by normal mode analysis. All calculations were carried out using the Gaussian 03 program.[68]

Results and discussion

The local structure of the isomorphously substituted MFI structure

Selected parameters of the active sites of both zeolites are listed in Table 1 and illustrated in Fig. 2a–b. It is obvious that the type of trivalent atom substituted into the zeolite framework has a significant effect on the structure of the zeolite framework and the length of the O–H bond of the Brønsted acid site. For the acid site structure, the O–H bond distance of the H-[B]-MFI zeolite is slightly shorter than that of the H-[Al]-MFI zeolite by 0.003 Å. The negligible difference of the O1–H1 bond distance has an effect on the charge-population changes for the H1 atom (0.5419 *vs.* 0.5755), suggesting that the acid site of the H-[Al]-MFI zeolite is more acidic than that of the H-[B]-MFI zeolite. Some significant differences are found in the bond distances and bond angles of the zeolite framework. The distances between the silicon atom and the bridging oxygen atom (Si–O bond distance) of the H-[B]-MFI zeolite are slightly longer than those of the H-[Al]-MFI zeolite and the angles between the substituted site and neighboring silicon atoms (M^{3+}–O–Si) in the H-[B]-MFI zeolite are larger than those in the [Al]-MFI by around 10–13°. The distances between the substituted site and the bridging oxygen atoms (M^{3+}–O) in the H-[B]-MFI are significantly shorter than those in the [Al]-MFI zeolite by 0.02 and 0.26 Å for the M^{3+}–O1 and M^{3+}–O2 bond distances, respectively. Because of the small size of the B^{3+} cation, the length of the B–O1 bond distance no bonding occurs between the B and the bridging hydroxyl group, and the structure is in the form of a trigonal BO_3 and a terminal silanol group is formed in the H-[B]-MFI zeolite. These observations are consistent with previous experimental and theoretical studies.[69–74]

Table 1 Optimized geometries and proton affinity (PA) of H-[B]-MFI and H-[Al]-MFI at the ONIOM2(B3LYP : 6-31G(d,p) : MNDO) scheme

Parameters	H-[B]-MFI	H-[Al]-MFI
O1–H1	0.970	0.973
Si1–O1	1.656	1.653
M^{3+}–O1	1.782	1.802
Si–O2	1.607	1.582
M^{3+}–O2	1.402	1.663
M–H	2.195	2.301
∠Si1–O1–M	137.6	127.8
∠Si2–O2–M	149.2	133.8
q(H1)[a]	0.5419	0.5755

[a] The atomic charges from the Mulliken population analysis were carried out by single point calculations with the full quantum calculation, HF/6-31G(d) level of theory.

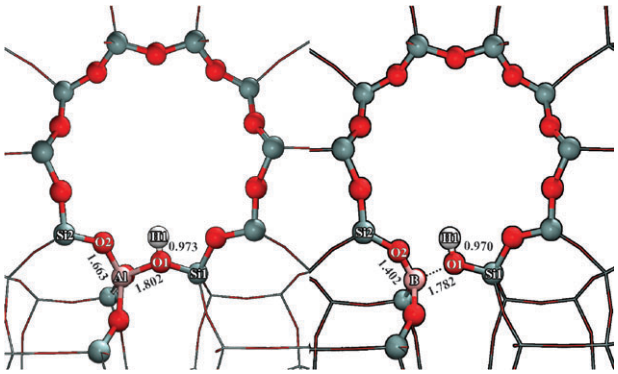

Fig. 2 Optimized geometric parameters of the 128T ONIOM model of zeolites at the B3LYP/6-31G(d,p) : MNDO scheme: (a) H-[Al]-MFI zeolite and (b) H-[B]-MFI zeolite.

The Beckmann rearrangement on an isomorphously substituted MFI structure

The 1,2 H-shift step. The geometrical parameters of the N-bound complex, the H-shift transition state and the O-bound complexes calculated by the ONIOM2 scheme are illustrated in Fig. 3a–c for the H-[Al]-MFI zeolite and Fig. 3d–f for the H-[B]-MFI zeolite. At the initial step, the cyclohexanone oxime molecule interacts with the acidic site of the zeolite *via* its nitrogen atom. The reaction subsequently proceeds in three consecutive steps. The first step is called 1,2 H-shift step. The initial adsorption complex; N-bound complex on both zeolites: H-[Al]-MFI and H-[B]-MFI zeolites, is in the form of a protonated complex, which is consistent with previous experimental studies[23,34] that observed the protonated form of cyclohexanone oxime over the Brønsted acid site. In both zeolitic systems, the O1–H1 bond in the N–bond complex is lengthened to 1.775 and 1.764 Å to form the N–H1 single bond. The N–H1 bond distance is predicted to be 1.035 and 1.043 Å for the H-[Al]-MFI and the H-[B]-MFI systems,

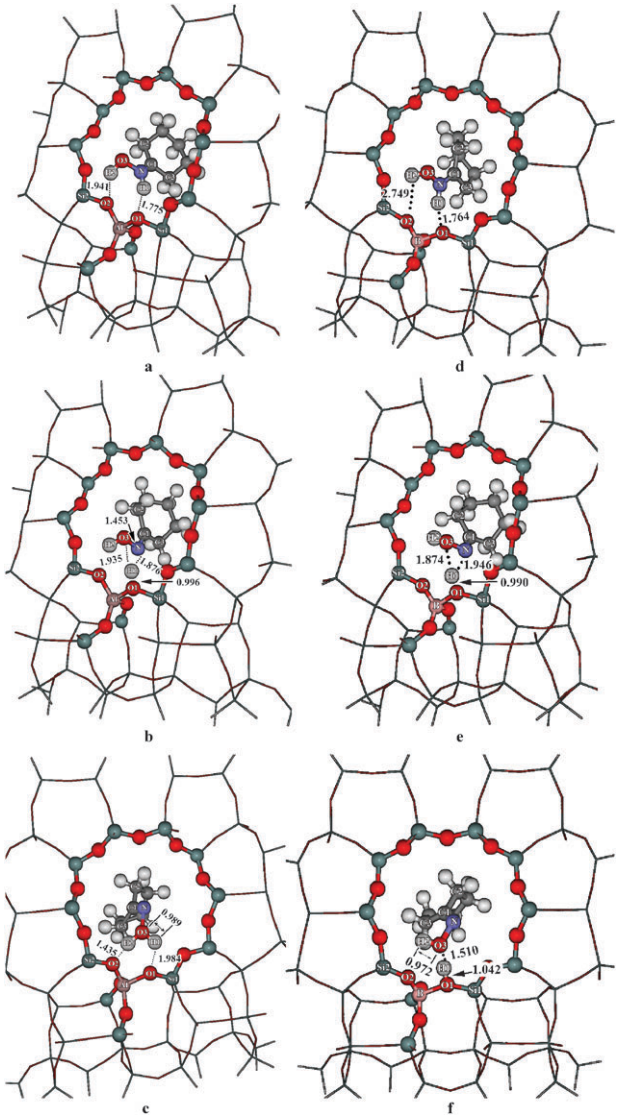

Fig. 3 Optimized geometrical parameters of the stationary points corresponding to 1,2 H-shift step of cyclohexanone oxime: (a) N-bound complex, (b) 1,2 H-shift transition state complex and (c) O-bound complex, respectively. They are catalyzed by the H-[Al]-MFI zeolite. Sections (d)–(f) present the corresponding complexes on the H-[B]-MFI zeolite.

respectively. This complex consists of the two strong hydrogen bond interactions between O5–H2–O2 and N–H1–O1 and corresponds to the previous theoretical studies on the MFI[26] and FAU[27] zeolites. The adsorption energy of this complex is calculated to be −50.67 and −39.91 kcal mol^{-1} for the H-[Al]-MFI and H-[B]-MFI systems, respectively. The difference of the adsorption energy of this complex is due mainly to the acidic strength of the Brønsted acid sites of both zeolites. Due to the H-[Al]-MFI zeolite being more acidic than the H-[B]-MFI zeolite, the adsorption energy of cyclohexanone oxime on the H-[Al]-MFI zeolite is more exothermic. The transition state (*cf.* Fig. 3b and e) of the first step is the transfer of the active proton (H1) from the nitrogen-ended site to the oxygen-ended site of the cyclohexanone oxime. The structural changing from the N-bound complex to the other one in this transition state can be observed from the N–H1, O3–H1 and N–O3 bond distances. At the TS, the N–O3 bond distance is elongated by about 0.08 and 0.06 Å for the H-[Al]-MFI and H-[B]-MFI systems, respectively. For the active H1 atom, the bond distance between it and the nitrogen atom is broken and located in the midway point between the N and O atoms, with the N–H1 and O3–H1 active distances being 1.876 and 1.935 Å for the H-[Al]-MFI system, and 1.946 and 1.874 Å for the H-[B]-MFI system. These distances correspond to a previous observation in the zeolitic systems: MOR[28] (1.90 Å), MFI[26] (1.95 Å) and FAU[27] (1.85 Å). With assistance from the zeolite framework in shuttling the proton, the barrier height of this step is 31.5 and 24.3 kcal mol^{-1} for the H-[Al]-MFI and H-[B]-MFI zeolites, respectively. They are quantitatively similar to the activation energies of the oximes in the zeolite systems in previous studies[26–28] by 21–31 kcal mol^{-1}. The reduction of the activation energy for this step in the H-[B]-MFI zeolite, as compared to that in the H-[Al]-MFI zeolite, is due mainly to the decrease of the acidity of Brønsted site of the zeolite that leads to a significantly weak interaction in the initial-state adsorption of reaction, N-bound complex. This observation is consistent with previous works,[26,27] concluding that the barrier height of this step corresponds to the strength of the adsorption in the N-bound complex. Subsequently, after the 1,2 H-shift process, the O-bound complex, which is an interaction between the oxygen atom of cyclohexanone oxime and the Brønsted acid site of zeolite, is formed with the adsorption energy of −31.51 and −18.91 kcal mol^{-1}. Contrary to the N-bound complex, it can be seen clearly from Fig. 3c and f that only the H-[Al]-MFI zeolite promotes the protonation of the O-bound complex, whereas the corresponding complex on the H-[B]-MFI system is in a molecularly adsorbed state. In the [Al]-MFI system, the protonated-oxygen cyclohexanone oxime interacts with the bridging oxygens of zeolite *via* two strong hydrogen bonds: O1···H1–O3 and O2···H2–O3 (1.984 and 1.435 Å), while for the [B]-MFI system, the physisorbed oxime molecule is stabilized by one strong O3···H1–O1 hydrogen bond (1.510 Å) and one weaker O2···H2–O3 hydrogen bond (2.414 Å). The difference between the geometrical O-bound complex and the calculated heat of adsorption values corresponds to the acidic strength of the Brønsted acid site of the zeolites.

The rearrangement step. The key parameters of the rearrangement transition state and the corresponding intermediate product are illustrated in Fig. 4a–b for the H-[Al]-MFI zeolite and Fig. 4c–d for the H-[B]-MFI, respectively. In the transition state of the [Al]-MFI zeolite, the C1–C2 bond is broken and the C2 is shifted toward the N atom and located above the C1–N bond, causing a shortening of the N–C1 bond distance from 1.280 to 1.187 Å. The bond distances of the C1–C2 and N–C2 bonds are predicted to be 1.864 and 1.995 Å, respectively. Concurrently with the breaking of the C1–C2 bond, the N–O3 bond is broken and a water molecule is separated from the rest of the molecules. The intermolecular N–O bond distance is significantly elongated to 2.545 Å. The O3–H1 and O3–H2 bond distances are shortened to 0.966 and 0.976, respectively, and the bond angle of H1–O2–H2 is slightly spread from 103.0 to 103.7°, while in the rearrangement TS step over the H-[B]-MFI zeolite, the

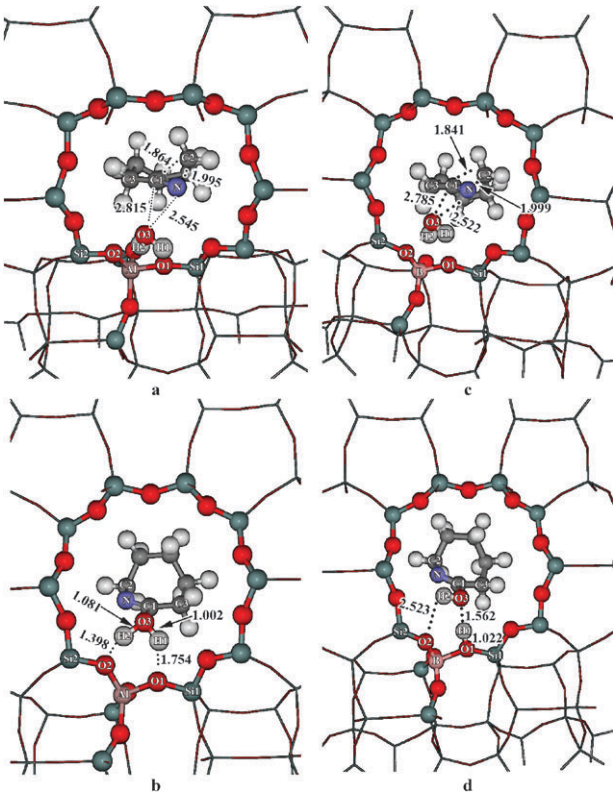

Fig. 4 Optimized geometrical parameters of the stationary points corresponding to the rearrangement step of cyclohexanone oxime: (a) the rearrangement transition state complex and (b) the enol–amide adsorption complex, respectively. Those are catalyzed by the H-[Al]-MFI zeolite. Sections (c) and (d) present the corresponding complexes on the H-[B]-MFI zeolite.

elimination of the C1–C2 bond and the transfer of the C2 to the N atom take place with low activation energy. The C2 atom is located in between the C1 atom and N atom with bond distances of 1.841 and 1.999 Å for the C1–C2 and N–C2 bond lengths, respectively. Furthermore, comparing the rearrangement transition state between both zeolitic systems, we found that the protonation occurred during the rearrangement in the H-[B]-MFI zeolite. The activation energy for this step is calculated to be 16.15 and 7.46 kcal mol^{-1} for the H-[Al]-MFI and the H-[B]-MFI zeolites, respectively. The reduction of the energy barrier for this step is due mainly to the adsorption strength of the O-bound complex. In the H-[B]-MFI zeolite, this complex is in the neutral form complex, whereas in the other zeolite, it is in the protonated complex. Therefore, the effects from the zeolite framework have a much larger degree of stabilization of the O-bound complex in the H-[Al]-MFI zeolite than that in the H-[B]-MFI zeolite. Our results compare well to the periodic calculation[28] that predicted the activation energies to be 21.05 and 15.31 kcal mol^{-1} for the 1,2 H-shift and rearrangement steps on the Brønsted acid site of MOR zeolite. After the rearrangement process, the enol–amide complex is formed. The distances of the forming bonds, N–C2 and C1–O3, are 1.465 and 1.469 Å, respectively, resulting in slight shortening of the N–C1 bond. The adsorbed complex is in a protonated form, forming two slightly stronger hydrogen bonds to the bridging oxygen atoms of zeolite with the $–OH_2$ group. The intermolecular O1–H1 and O2–H2 bond distances are 1.754 and 1.398 Å, respectively. In the H-[B]-MFI zeolite, the enol–amide complex is in the neutral complex consisting of only a strong hydrogen bond between the O3 atom and the Brønsted acid site of [B]-MFI zeolite. The distances of the newly formed N–C2, C1–O3 and O3–H1 bonds are 1.460, 1.402 and 1.562 Å, respectively. The adsorption energies are predicted to be −59.86 and −52.19 kcal mol^{-1} for H-[Al]-MFI and H-[B]-MFI zeolites, respectively. The difference in the adsorption energies of these complexes is in agreement with their structural adsorption complexes, as shown in Fig. 4b and d.

Tautomerization step. The optimized structures of this state are illustrated in Fig. 5a–b for H-[Al]-MFI zeolite and Fig. 5c–d for H-[B]-MFI, respectively. The transition state of this step (*cf*. Fig. 5a and c) is the migration of the H atom from the –OH group to the N atom to form the ε-caprolactam. In the H-[Al]-MFI system, the migrating proton (H2) is close to the midway point between the O3 and N atoms (the distances of O3–H2 and N–H2 bonds are 1.218 and 1.414 Å) where it is nearly in the same plane with the O3 and N atoms of the enol–amide complex (the N–C1–O3–H2 dihedral angle is 3.0°; see Fig. 5a and c). These take place simultaneously with shortening of the C–O bond (by about 0.05 Å) and the slight elongation of the N–C1 bond (by about 0.02 Å) for transferring to the amide compound, the keto–amide complex. Whilst in the H-[B]-MFI zeolite, the migration proton is located in a

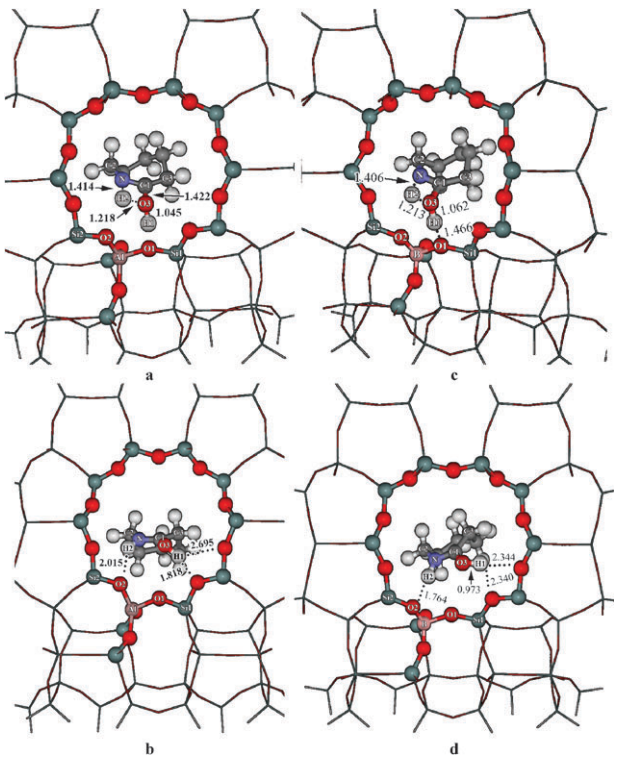

Fig. 5 Optimized geometric parameters of the complexes corresponding to the tautomerization step of cyclohexanone oxime: (a) the tautomerization transition state complex and (b) the keto–amide adsorption complex, respectively. Those are catalyzed by the H-[Al]-MFI zeolite. Sections (c) and (d) present the corresponding complexes on the H-[B]-MFI zeolite.

similar geometry as that found in the H-[Al]-MFI zeolite. The N–H2 and O3–H2 bond distances are 1.406 and 1.213 Å, respectively. These are quantitatively similar to the corresponding bonds in the H-[Al]-MFI zeolite. Concurrently with the migration of the H2 atom, the proton of the Brønsted acid site is transferred to protonate the O2 atom of the enol–amide complex during the transition state. The activation energy for this step, using the embedded-ONIOM2 model, is evaluated to be 18.95 and 20.43 kcal mol^{-1} for the H-[Al]-MFI and H-[B]-MFI zeolites, respectively. The barrier for this step in the H-[Al]-MFI zeolite is slightly lower than that in the H-[B]-MFI zeolite because of the enhancement of the acidity of the H2 atom caused by the protonation at the oxygen atom of the enol–amide product. After the tautomerization process, the keto–amide product or ε-caprolactam is formed (*cf*. Fig. 5b and d). The interaction between the keto–amide complex and the Brønsted acid site of both zeolites is in the form of a protonated complex which agrees well with the experiment observation[34,37] that the O-protonated ε-caprolactam is formed over the Brønsted acid sites of zeolite. The desorption energy of the ε-caprolactam molecule is calculated to be −44.96 and −39.11 kcal mol^{-1} for the H-[Al]-MFI and H-[B]-MFI zeolites, respectively. The high value of the desorption energy indicates that the desorbing process of the reaction product from the zeolites possibly obstructs the adsorption of the oxime molecule in the first step of the reaction. These results agree well with previous experimental studies,[14,15] concluding that the reaction on the strong Brønsted acid of MFI is very active in the rearrangement of the cyclohexanone oxime to the ε-caprolactam, but a problem will be encountered due to a difficulty in the desorption step, which also leads to the catalyst deactivation because of coke deposition in the zeolite pores. Because the produced ε-caprolactam remains on the acid sites, it is converted to an oligomer, which could be a precursor of coke.

A comparison of the results of the embedded ONIOM model and the bare cluster model (see ESI),† reveals that the effects from the zeolite framework play an important role in lowering the activation energies in each step of the reaction, excepting the 1,2 H-shift step. It is because of the zeolite framework effect having a much larger degree of stabilization of the adsorption complex, N-bound complex, than at the TS complex. Consequently, this step is the rate-determining step of the reaction in both zeolites which have activation energies of 31.46 and 24.33 kcal mol^{-1} for the H-[Al]-MFI and H-[B]-MFI zeolites, respectively (*cf*. Fig.6). The largest effect is at the rearrangement step, which is the connection between the O-bound complex and the enol–amide complex. The zeolite framework effects lower the energy barrier by about 10 and 25 kcal mol^{-1} for the H-[Al]-MFI and H-[B]-MFI zeolites, respectively.

Conclusions

In this work, we have examined both the role of acid strength and the zeolite framework effects on the Beckmann rearrangement of cyclohexanone oxime catalyzed by the isomorphously substituted MFI zeolites: the H-[Al]-MFI and the H-[B]-MFI zeolites. All of these systems have been investigated by both the bare cluster and the ONIOM2 scheme. By use of the ONIOM2 scheme in combination with the electrostatic potential

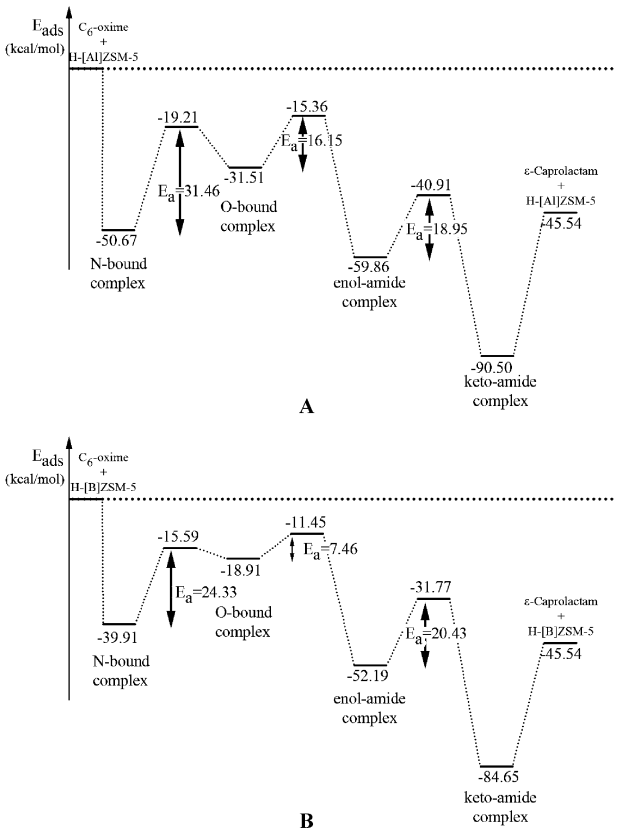

Fig. 6 The energetic profile along the pathway of the Beckmann rearrangement of the cyclohexanone oxime molecule on zeolites at the embedded ONIOM2 scheme (MP2/6-311G(d,p):HF/6-31G(d)//B3LYP/6-31G(d,p):MNDO) level of theory: (a) H-[Al]-MFI zeolite, (b) H-[B]-MFI zeolite. The energetic changes for complexes are in kcal mol^{-1}.

obtained from the SCREEP method, it demonstrates that the electrostatic potential from the extended zeolite framework plays a dominant function in the reduction of the energy barrier. The reaction is initiated by the strong interaction of the N-ended cyclohexanone oxime on the acid sites of the zeolite. The N-ended adsorption complex is transformed to the O-ended adsorption complex *via* the 1,2 H-shift step. Subsequently, the ε-caprolactam is yielded rapidly *via* the rearrangement step and the tautomerization step, respectively. From the embedded ONIOM2 scheme, the rate determining step of the reaction is the 1,2 H-shift step which has an energy barrier of 31.46 and 24.33 kcal mol^{-1} for the H-[Al]-MFI and the H-[B]-MFI zeolites, respectively (*cf*. Fig.6). Furthermore, we found that the protonation of the reaction product ε-caprolactam occurs in both zeolites H-[Al]-MFI and H-[B]-MFI. This leads to a strong adsorption on the catalyst surface. It should be noted that the catalyst deactivation might take place due to the irreversibly adsorbed ε-caprolactam molecule. One may expect that the addition of diluting solvents may play a crucial role in the desorption of the products from the zeolite micorpores, and, consequently, decrease the deactivation of the catalyst.

Acknowledgements

This work was supported in part by grants from the Thailand Research Fund (to J.S. and J.L.) and the Science Research

Fund (ScRF) from the Faculty of Science, Kasetsart University (to J.S.) as well as the Commission of Higher Education, Ministry of Education under Postgraduate Education and Research Programs in Petroleum and Petrochemicals, and Advanced Materials. Support from the National Nanotechnology Center (NANOTEC Center of excellence and CNC) under the National Science and Technology Development Agency is also acknowledged.

References

1 E. Beckmann, *Chem. Ber*., 1886, **19**, 988–993.
2 A. H. Blatt, *Chem. Rev*., 1933, **12**, 215–260.
3 B. Jones, *Chem. Rev*., 1944, **35**, 335–350.
4 H. E. Ungnade and D. A. McLaren, *J. Org. Chem*., 1945, **10**, 29–33.
5 D. E. Pearson and J. D. Bruton, *J. Org. Chem*., 1954, **19**, 957–963.
6 W. Z. Heldt, *J. Org. Chem*., 1961, **26**, 1695–1702.
7 H. Ichihashi and H. Sato, *Appl. Catal., A*, 2001, **221**, 359–366.
8 Y. Izumi, H. Ichihashi, Y. Shimazu, M. Kitamura and H. Sato, *Bull. Chem. Soc. Jpn*., 2007, **80**, 1280–1287.
9 H. Ichihashi, M. Ishida, A. Shiga, M. Kitamura, T. Suzuki, K. Suenobu and K. Sugita, *Catal. Surveys Asia*, 2003, **7**, 261–270.
10 C. Flego and L. Dalloro, *Microporous Mesoporous Mater*., 2003, **60**, 263–271.
11 G. P. Heitmann, G. Dahlhoff and W. F. Holderich, *J. Catal*., 1999, **186**, 12–19.
12 G. P. Heitmann, G. Dahlhoff, J. P. M. Niederer and W. F. Holderich, *J. Catal*., 2000, **194**, 122–129.
13 H. Ichihashi and M. Kitamura, *Catal. Today*, 2002, **73**, 23–28.
14 T. Takahashi, T. Kai and E. Nakao, *Appl. Catal., A*, 2004, **262**, 137–142.
15 P. O'Sullivan, L. Forni and B. K. Hodnett, *Ind. Eng. Chem. Res*., 2001, **40**, 1471–1475.
16 T. Takahashi, M. N. A. Nasution and T. Kai, *Appl. Catal., A*, 2001, **210**, 339–344.
17 L. Dai, K. Koyama, M. Miyamoto and T. Tatsumi, *Appl. Catal., A*, 1999, **189**, 237–242.
18 C. Ngamcharussrivichai, P. Wu and T. Tatsumi, *Chem. Lett*., 2004, **33**, 1288–1289.
19 C. Ngamcharussrivichai, P. Wu and T. Tatsumi, *Appl. Catal., A*, 2005, **288**, 158–168.
20 L.-X. Dai, Y. Iwaki, K. Koyama and T. Tatsumi, *Appl. Surf. Sci*., 1997, **121/122**, 335–338.
21 G. P. Heitmann, G. Dahlhoff and W. F. Holderich, *Appl. Catal., A*, 1999, **185**, 99–108.
22 Y.-M. Chung and H.-K. Rhee, *J. Mol. Catal. A: Chem*., 2000, **159**, 389–396.
23 Y. M. Chung and H. K. Rhee, *J. Mol. Catal. A: Chem*., 2001, **175**, 249–257.
24 Y. Zhang, Y. Wang and Y. Bu, *Microporous Mesoporous Mater*., 2008, **107**, 247–251.
25 P. Botella, A. Corma, S. Iborra, R. Monton, I. Rodriguez and V. Costa, *J. Catal*., 2007, **250**, 161–170.
26 J. Sirijaraensre, T. N. Truong and J. Limtrakul, *J. Phys. Chem. B*, 2005, **109**, 12099–12106.
27 J. Sirijaraensre and J. Limtrakul, *ChemPhysChem*, 2006, **7**, 2424–2432.
28 T. Bucko, J. Hafner and L. Benco, *J. Phys. Chem. A*, 2004, **108**, 11388–11397.
29 C. Ngamcharussrivichai, P. Wu and T. Tatsumi, *J. Catal*., 2005, **235**, 139–149.
30 A. Fernandez, A. Marinas, T. Blasco, V. Fornes and A. Corma, *J. Catal*., 2006, **243**, 270–277.
31 M. A. Camblor, A. Corma, H. Garcia, V. Semmer-Herledan and S. Valencia, *J. Catal*., 1998, **177**, 267–272.
32 B. Bonelli, L. Forni, A. Aloise, J. B. Nagy, G. Fornasari, E. Garrone, A. Gedeon, G. Giordano and F. Trifiro, *Microporous Mesoporous Mater*., 2007, **101**, 153–160.
33 L. Forni, E. Patriarchi, G. Fornasari, F. Trifiro, A. Katovic, G. Giordano and B. Nagy, *Stud. Surf. Sci. Catal*., 2005, **155**, 281–290.
34 V. R. R. Marthala, Y. Jiang, J. Huang, W. Wang, R. Glaeser and M. Hunger, *J. Am. Chem. Soc*., 2006, **128**, 14812–14813.
35 G. A. Fois, G. Ricchiardi, S. Bordiga, C. Busco, L. Dalloro, G. Spano and A. Zecchina, *Stud. Surf. Sci. Catal*., 2001, **135**, 2477–2484.
36 A. B. Fernandez, M. Boronat, T. Blasco and A. Corma, *Angew. Chem., Int. Ed*., 2005, **44**, 2370–2373.
37 A. B. Fernandez, I. Lezcano-Gonzalez, M. Boronat, T. Blasco and A. Corma, *J. Catal*., 2007, **249**, 116–119.
38 J. M. Vollmer, E. V. Stefanovich and T. N. Truong, *J. Phys. Chem. B*, 1999, **103**, 9415–9422.
39 I. H. Hillier, *THEOCHEM*, 1999, **463**, 45–52.
40 E. V. Stefanovich and T. N. Truong, *J. Phys. Chem. B*, 1998, **102**, 3018–3022.
41 J. Limtrakul, S. Jungsuttiwong and P. Khongpracha, *J. Mol. Struct*., 2000, **525**, 153–162.
42 J. Limtrakul, P. Khongpracha, S. Jungsuttiwong and T. N. Truong, *J. Mol. Catal. A: Chem*., 2000, **153**, 155–163.
43 J. Limtrakul, T. Nanok, S. Jungsuttiwong, P. Khongpracha and T. N. Truong, *Chem. Phys. Lett*., 2001, **349**, 161–166.
44 J. Limtrakul, S. Nokbin, P. Chuichay, P. Khongpracha, S. Jungsuttiwong and T. N. Truong, *Stud. Surf. Sci. Catal*., 2001, **135**, 2469–2476.
45 P. Treesukol, K. Srisuk, J. Limtrakul and T. N. Truong, *J. Phys. Chem. B*, 2005, **109**, 11940–11945.
46 S. Jungsuttiwong, J. Limtrakul and T. N. Truong, *J. Phys. Chem. B*, 2005, **109**, 13342–13351.
47 M. Sierka and J. Sauer, *J. Phys. Chem. B*, 2001, **105**, 1603–1613.
48 M. E. Franke, M. Sierka, U. Simon and J. Sauer, *Phys. Chem. Chem. Phys*., 2002, **4**, 5207–5216.
49 O. Bludsky, M. Silhan, P. Nachtigall, T. Bucko, L. Benco and J. Hafner, *J. Phys. Chem. B*, 2005, **109**, 9631–9638.
50 K. Bobuatong and J. Limtrakul, *Appl.Catal., A*, 2003, **253**, 49–64.
51 S. Kasuriya, S. Namuangruk, P. Treesukol, M. Tirtowidjojo and J. Limtrakul, *J. Catal*., 2003, **219**, 320–328.
52 S. Namuangruk, P. Pantu and J. Limtrakul, *J. Catal*., 2004, **225**, 523–530.
53 S. Pabchanda, P. Pantu and J. Limtrakul, *J. Mol. Catal. A: Chem*., 2005, **239**, 103–110.
54 W. Panjan and J. Limtrakul, *J. Mol. Struct*., 2003, **654**, 35–45.
55 P. Pantu, S. Pabchanda and J. Limtrakul, *ChemPhysChem*, 2004, **5**, 1901–1906.
56 C. Raksakoon and J. Limtrakul, *THEOCHEM*, 2003, **631**, 147–156.
57 R. Rungsirisakun, B. Jansang, P. Pantu and J. Limtrakul, *J. Mol. Struct*., 2004, **733**, 239–246.
58 W. Sangthong, M. Probst and J. Limtrakul, *J. Mol. Struct*., 2005, **748**, 119–127.
59 X. Solans-Monfort, M. Sodupe, V. Branchadell, J. Sauer, R. Orlando and P. Ugliengo, *J. Phys. Chem. B*, 2005, **109**, 3539–3545.
60 P. Pantu, B. Boekfa, B. Sunpetch and J. Limtrakul, *Chem. Eng. Commun*., 2008, **195**, 1477–1485.
61 B. Jansang, T. Nanok and J. Limtrakul, *J. Phys. Chem. C*, 2008, **112**, 540–547.
62 W. Panyaburapa, T. Nanok and J. Limtrakul, *J. Phys. Chem. C*, 2007, **111**, 3433–3441.
63 P. Pantu, B. Boekfa and J. Limtrakul, *J. Mol. Catal. A: Chem*., 2007, **277**, 171–179.
64 J. Lomratsiri, M. Probst and J. Limtrakul, *J. Mol. Graphics Modell*., 2006, **25**, 219–225.
65 B. Jansang, T. Nanok and J. Limtrakul, *J. Mol. Catal. A: Chem*., 2007, **264**, 33–39.
66 N. Injan, N. Pannorad, M. Probst and J. Limtrakul, *Int. J. Quantum Chem*., 2005, **105**, 898–905.
67 B. Jansang, T. Nanok and J. Limtrakul, *J. Phys. Chem. B*, 2006, **110**, 12626–12631.
68 M. J. Frisch, G. W. Trucks, H. B. Schlegel, G. E. Scuseria, M. A. Robb, J. R. Cheeseman, J. J. A. Montgomery, T. Vreven, K. N. Kudin, J. C. Burant, J. M. Millam, S. S. Iyengar, J. Tomasi, V. Barone, B. Mennucci, M. Cossi, G. Scalmani, N. Rega, G. A. Petersson, H. Nakatsuji, M. Hada, M. Ehara, K. Toyota, R. Fukuda, J. Hasegawa, M. Ishida, T. Nakajima, Y. Honda, O. Kitao, H. Nakai, M. Klene, X. Li, J. E. Knox, H. P. Hratchian,

J. B. Cross, V. Bakken, C. Adamo, J. Jaramillo, R. Gomperts, R. E. Stratmann, O. Yazyev, A. J. Austin, R. Cammi, C. Pomelli, J. W. Ochterski, P. Y. Ayala, K. Morokuma, G. A. Voth, P. Salvador, J. J. Dannenberg, V. G. Zakrzewski, S. Dapprich, A. D. Daniels, M. C. Strain, O. Farkas, D. K. Malick, A. D. Rabuck, K. Raghavachari, J. B. Foresman, J. V. Ortiz, Q. Cui, A. G. Baboul, S. Clifford, J. Cioslowski, B. B. Stefanov, G. Liu, A. Liashenko, P. Piskorz, I. Komaromi, R. L. Martin, D. J. Fox, T. Keith, M. A. Al-Laham, C. Y. Peng, A. Nanayakkara, M. Challacombe, P. M. W. Gill, B. Johnson, W. Chen, M. W. Wong, C. Gonzalez and J. A. Pople, *GAUSSIAN 03*, Gaussian, Inc., Wallingford CT, 2004.

69 L. Regli, S. Bordiga, C. Lamberti, K. P. Lillerud, S. I. Zones and A. Zecchina, *J. Phys. Chem. C*, 2007, **111**, 2992–2999.

70 Y. Wang, D. Zhou, G. Yang, S. Miao, X. Liu and X. Bao, *J. Phys. Chem. A*, 2004, **108**, 6730–6734.

71 S. P. Yuan, J. G. Wang, Y. W. Li and H. Jiao, *THEOCHEM*, 2004, **674**, 267–274.

72 S. P. Yuan, J. G. Wang, Y. W. Li and H. Jiao, *J. Phys. Chem. A*, 2002, **106**, 8167–8172.

73 R. C. Deka, N. Tajima and K. Hirao, *THEOCHEM*, 2001, **535**, 31–38.

74 H. Berndt, A. Martin, H. Kosslick and B. Luecke, *Microporous Mater.*, 1994, **2**, 197–204.